Electronic Supplementary Information

Controlled molecular assemblies of chiral boron dipyrromethene derivatives for circularly polarized luminescence in the red and near-infrared regions

Hayato Sakai,[*a] Yudai Suzuki,[a] Makoto Tsurui,[b] Yuichi Kitagawa,[b] Takuya Nakashima,[cd] Tsuyoshi Kawai,[d] Yuta Kondo,[e] Go Matsuba,[e] Yasuchika Hasegawa[*b] and Taku Hasobe[*a]

[a]Department of Chemistry, Faculty of Science and Technology, Keio University, 3-14-1 Hiyoshi, Yokohama, Kanagawa 223-8522 Japan.

[b]Faculty of Engineering and Institute for Chemical Reaction Design and Discovery (WPI-ICReDD), Hokkaido University, Sapporo, Hokkaido 060-8628, Japan.

[c]Department of Chemistry, Graduate School of Science, Osaka Metropolitan University, Sumiyoshi, Osaka 558-8585, Japan.

[d]Graduate School of Materials Science, Nara Institute of Science and Technology, Ikoma, Nara 630-0192 Japan.

[e]Graduate School of Organic Materials Science, Yamagata University, Yonezawa, Yamagata 992-8510, Japan.

Experimental

X-ray Diffraction Measurements. X-ray diffraction (XRD) measurements were carried out with a D8 ADVANCE (Bruker) using Ni-filtered Cu Kα line radiation (λ = 1.5418 Å). The accelerating voltage was set at 40 kV with 20 mA current, and profiles were collected in the $5° < 2\theta < 40°$ range with a step size of 0.03°.

Small-angle X-ray scattering (SAXS) measurements. Small-angle X-ray scattering (SAXS) measurements were carried out with beam-line BL6A, Photon Factory, KEK, Japan (Proposal No. 21G524 and 22G027).

. The scattering vector, q, is defined as

$$q = \frac{4\pi}{\lambda}\sin\theta \qquad (1),$$

where 2θ and λ are the scattering angle and wavelength (1.5 Å), respectively. The camera lengths was 2410 mm. A PILATUS 2M detector (Dectris AG, Baden, Switzerland) detector was used with a q range of 0.07 to 2.0 nm^{-1}. Data processing, which included controlling the contrast of the 2D-patterns and the preparation of a 1D-profile from the obtained 2D-patterns, was performed using the FIT-2D software (Ver. 12.077, Andy Hammersley/ESRF, Grenoble, France).

Synthesis

Scheme S1. Synthetic Scheme of *R*-0Ph-B-BODIPY.

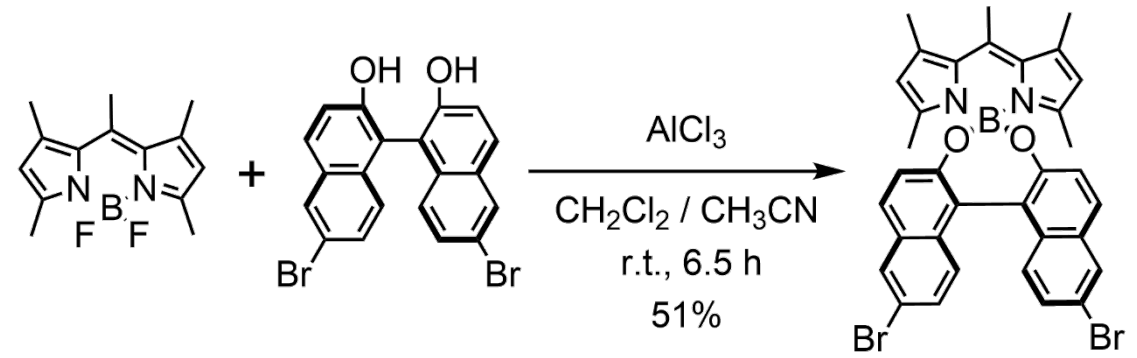

Synthesis of *R*-0Ph-B-BODIPY. BODIPY-ref (100 mg, 0.38 mmol), $AlCl_3$ (76 mg, 0.57 mmol) were dissolved in CH_2Cl_2 (10 ml) and refluxed for 30 min. After cooling down to room temperature, enantiopure *R*-Br-BINOL (337 mg, 0.76 mmol) in acetonitrile (5 ml) was added dropwise and stirred at room temperature for 6 h. Next, the solvent was washed with saturated NaCl aqueous solution, dried over anhydrous $MgSO_4$ and evaporated. Finally, the crude was purified by chromatography on silica gel eluting with hexane/CH_2Cl_2 (1/1, v/v) and enantiopure *R*-0Ph-B-BODIPY (yield: 120 mg, 51%) was obtained. *S*-0Ph-B-BODIPY was synthesized by changing from enantiopure *R*-Br-BINOL to enantiopure *S*-Br-BINOL. ^{1}H NMR ($CDCl_3$) δ: 7.96 (2H, s), 7.65 (2H, d, J = 10.0 Hz), 7.21 (2H, d, J = 8.6 Hz), 7.14 (2H, d, J = 8.6 Hz), 7.02 (2H, d, J = 8.1 Hz), 5.86 (2H, s), 2.67 (3H, s), 2.43 (6H, s), 1.67 (6H, s). ^{13}C-NMR ($CDCl_3$) δ: 154.87 (s), 154.36 (s), 141.19 (s), 140.80 (s), 133.01 (s), 132.06 (s), 130.94 (s), 129.82 (s), 128.62 (s), 128.54 (s), 128.32 (s), 124.94 (s), 122.18 (s), 120.94 (s), 117.08 (s), 17.66 (s), 16.95 (s), 15.96 (s). High resolution MALDI−TOF MS: m/z calcd, 664.0532; found, 664.0515 [M].

Scheme S2. Synthetic Scheme of *R*-1Ph-BODIPY.

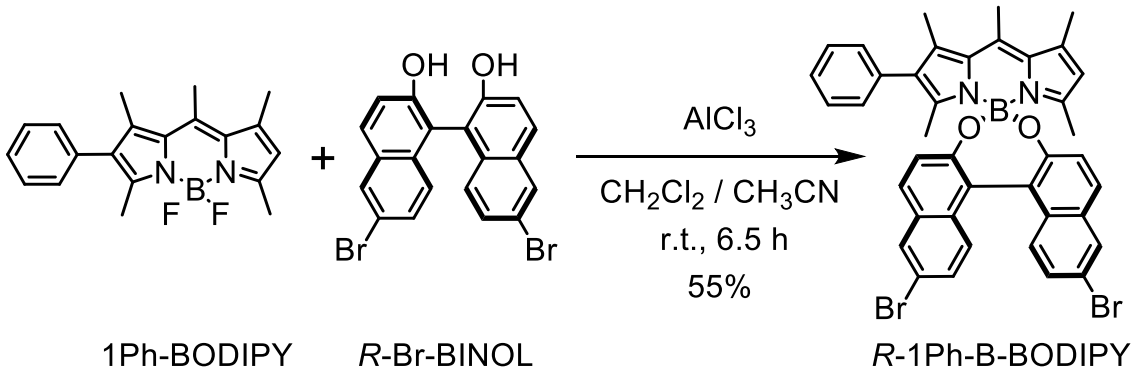

Synthesis of *R*-1Ph-B-BODIPY. 1Ph-BODIPY (100 mg, 0.30 mmol), $AlCl_3$ (59 mg, 0.44 mmol) were dissolved in CH_2Cl_2 (10 ml) and refluxed for 30 min. After cooling down to room temperature, enantiopure *R*-Br-BINOL (261 mg, 0.59 mmol) in acetonitrile (5 ml) was added dropwise and stirred at room temperature for 6 h. Next, the solvent was washed with saturated NaCl aqueous solution, dried over anhydrous $MgSO_4$ and evaporated. Finally, the crude was purified by chromatography on silica gel eluting with hexane/CH_2Cl_2 (1/1, v/v) and enantiopure *R*-1Ph-B-BODIPY (yield: 115 mg, 55%) was obtained. *S*-1Ph-B-BODIPY was synthesized by changing from enantiopure *R*-Br-BINOL to enantiopure *S*-Br-BINOL. ^{1}H NMR ($CDCl_3$) δ: 7.96 (2H, s), 7.67 (1H, d, J = 8.8 Hz), 7.64 (1H, d, J = 8.8 Hz), 7.35-7.26 (3H, m), 7.23 (3H, d, J = 8.8 Hz), 7.21-7.17 (2H, m), 7.10 (1H, d, J = 8.8 Hz), 7.04-6.99 (4H, m), 5.85 (1H, s), 2.74 (3H, s), 2.45 (3H, s), 2.33 (3H, s), 1.71 (3H, s), 1.64 (3H, s). ^{13}C NMR ($CDCl_3$) δ: 154.82 (s), 154.75 (s), 152.51 (s), 141.38 (s), 140.87 (s), 137.08 (s), 133.91 (s), 133.42 (s), 132.82 (s), 132.10 (s), 132.01 (s), 131.07 (s), 130.80 (s), 130.35 (s), 129.84 (s), 129.69 (s), 129.49 (s), 128.65 (s), 128.57 (s), 128.54 (s), 128.50 (s), 128.40 (s), 128.16 (s), 127.80 (s), 127.70 (s), 126.91 (s), 125.05 (s), 124.72 (s), 122.21 (s), 121.31 (s), 120.48 (s), 117.16 (s), 117.08 (s), 17.71 (s), 17.47 (s), 15.79 (s), 15.73 (s), 14.94 (s). High resolution MALDI−TOF MS: m/z calcd, 740.0845; found, 740.0842 [M].

Scheme S3. Synthetic Scheme of *R*-2Ph-B-BODIPY

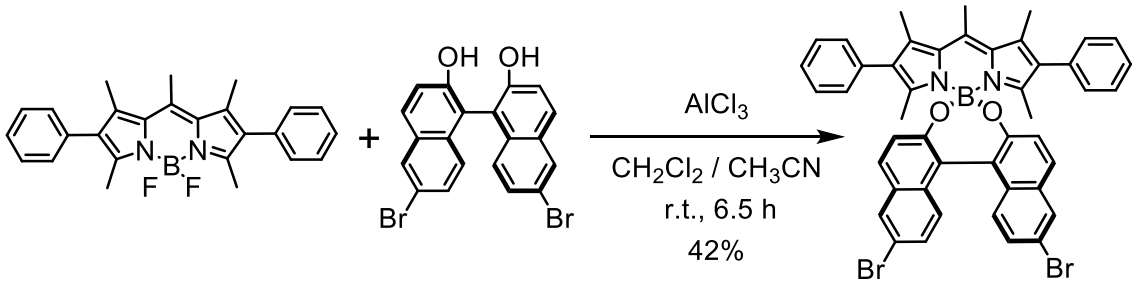

2Ph-BODIPY *R*-Br-BINOL *R*-2Ph-B-BODIPY

Synthesis of *R*-2Ph-B-BODIPY. 2Ph-BODIPY (100 mg, 0.24 mmol), $AlCl_3$ (50 mg, 0.37 mmol) were dissolved in CH_2Cl_2 (10 ml) and refluxed for 30 min. After cooling down to room temperature, enantiopure *R*-Br-BINOL (250 mg, 0.56 mmol) in acetonitrile (5 ml) was added dropwise and stirred at room temperature for 6 h. Next, the solvent was washed with saturated NaCl aqueous solution, dried over anhydrous $MgSO_4$ and evaporated. Finally, the crude was purified by chromatography on silica gel eluting with hexane/CH_2Cl_2 (1/1, v/v) and enantiopure *R*-2Ph-B-BODIPY (yield: 127 mg, 42%) was obtained. *S*-2Ph-B-BODIPY was synthesized by changing from enantiopure *R*-Br-BINOL to enantiopure *S*-Br-BINOL.^{1}H NMR ($CDCl_3$) δ: 7.96 (2H, s), 7.66 (2H, d, J = 8.6 Hz), 7.33-7.31 (4H, m), 7.27-7.24 (3H, m), 7.19-7.17 (3H, m), 7.01 (2H, d, J = 9.1 Hz), 6.96 (4H, d, J = 7.2 Hz), 2.81 (3H, s), 2.35 (6H, s), 1.68 (6H, s). ^{13}C NMR ($CDCl_3$) δ: 154.66 (s), 153.05 (s), 141.60 (s), 137.24 (s), 133.99 (s), 133.90 (s), 133.30 (s), 132.08 (s), 130.98 (s), 130.36 (s), 129.74 (s), 128.62 (s), 128.58 (s), 128.26 (s), 128.20 (s), 126.97 (s), 124.86 (s), 120.92 (s), 117.18 (s), 17.94 (s), 15.80 (s), 14.78 (s). High resolution MALDI−TOF MS: m/z calcd, 816.1158; found, 816.1168 [M].

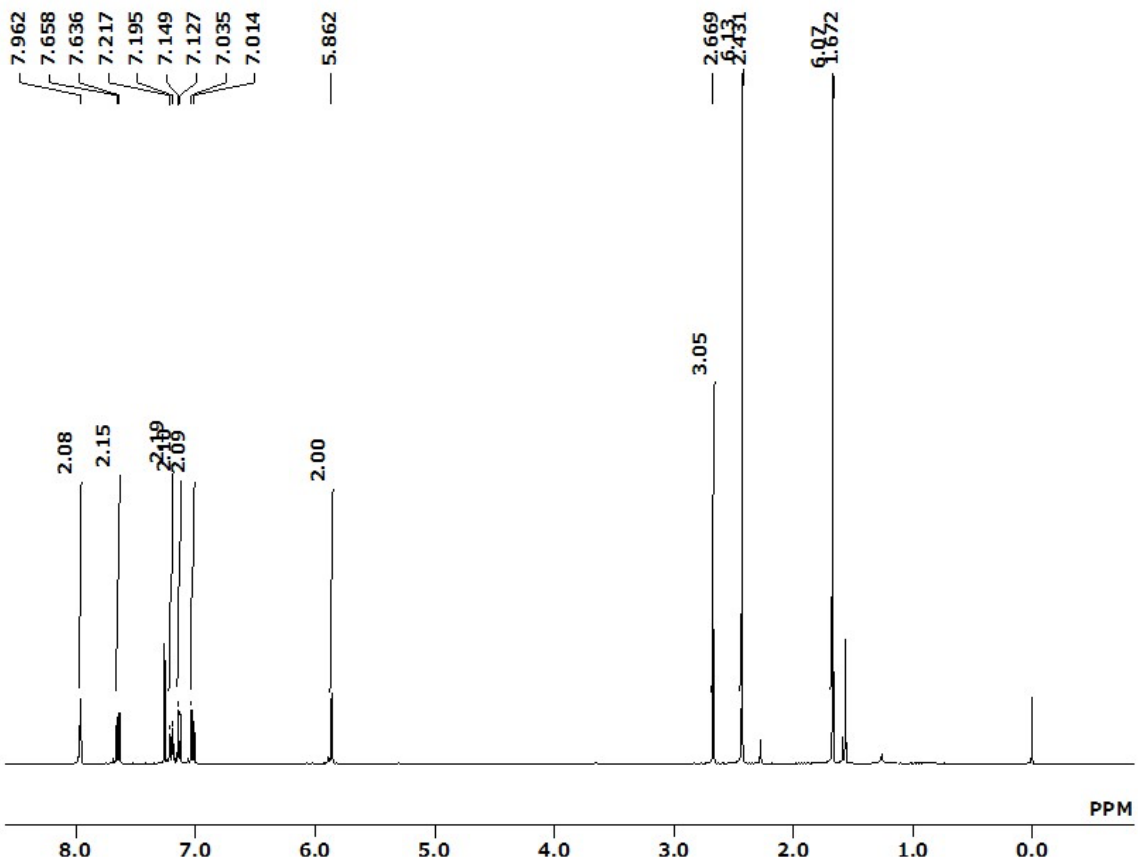

Fig. S1 ^{1}H NMR spectrum of *R*-0Ph-B-BODIPY.

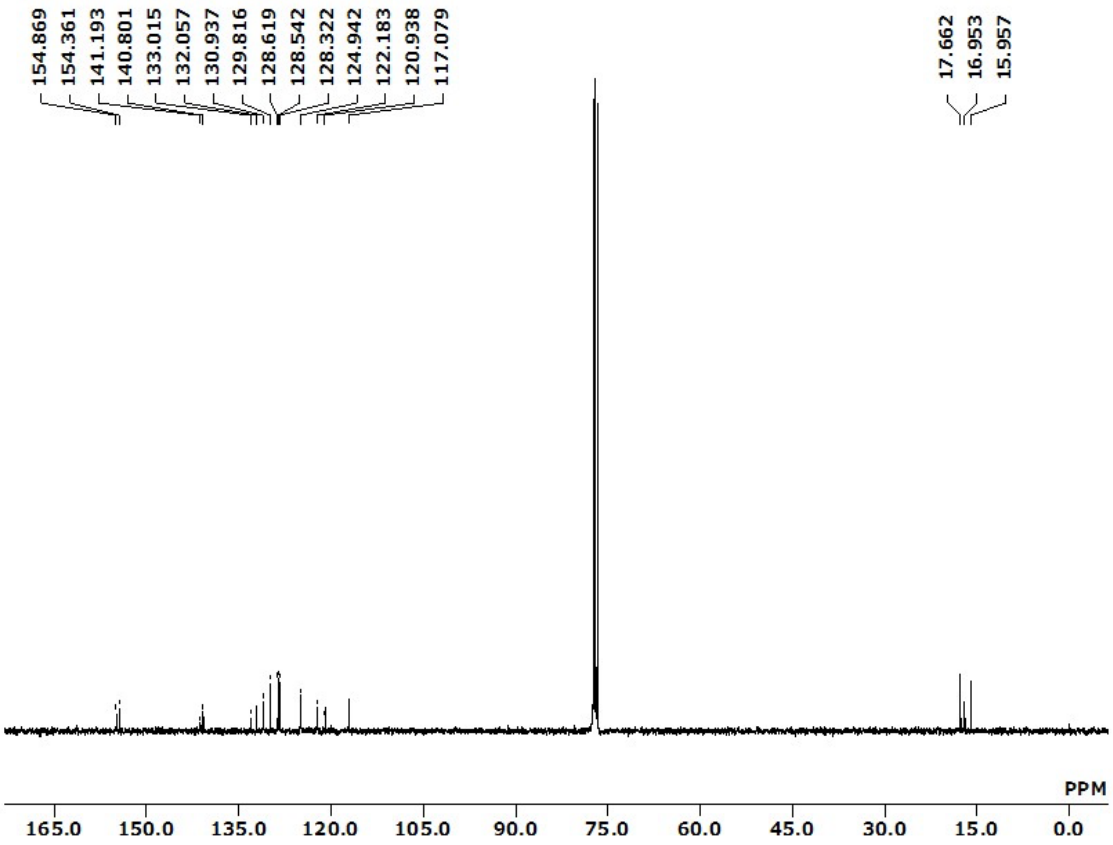

Fig. S2 ^{13}C NMR spectrum of *R*-0Ph-B-BODIPY.

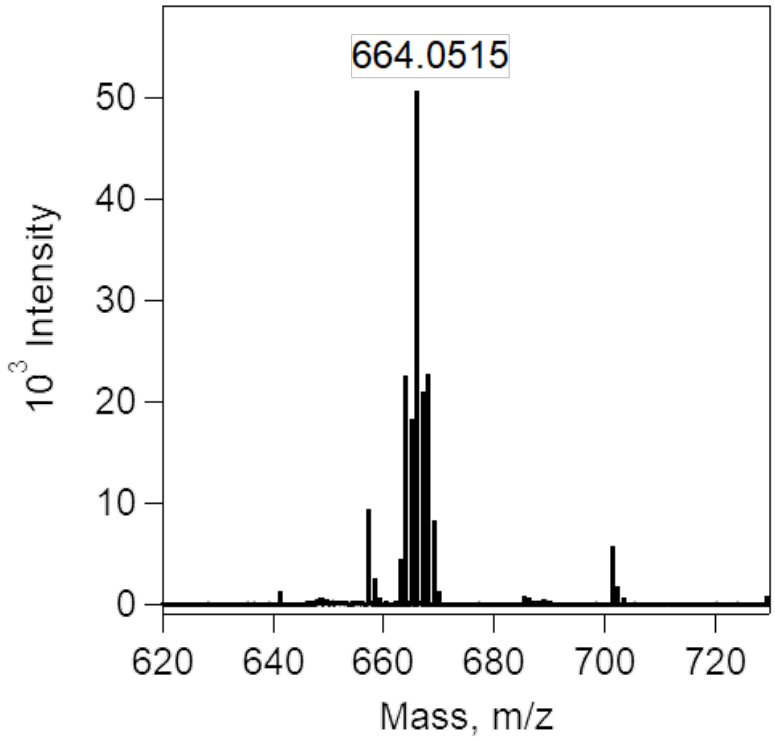

Fig. S3 High resolution MALDI−TOF MS spectrum of *R*-0Ph-B-BODIPY.

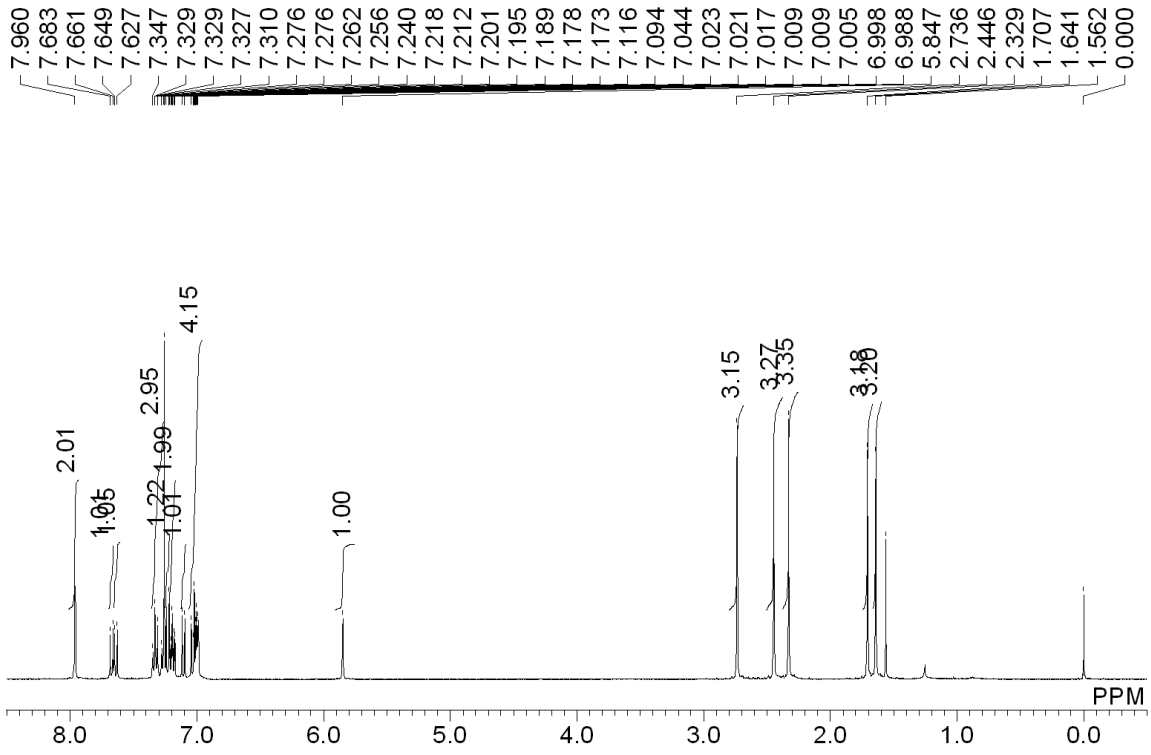

Fig. S4 ^{1}H NMR spectrum of *R*-1Ph-B-BODIPY.

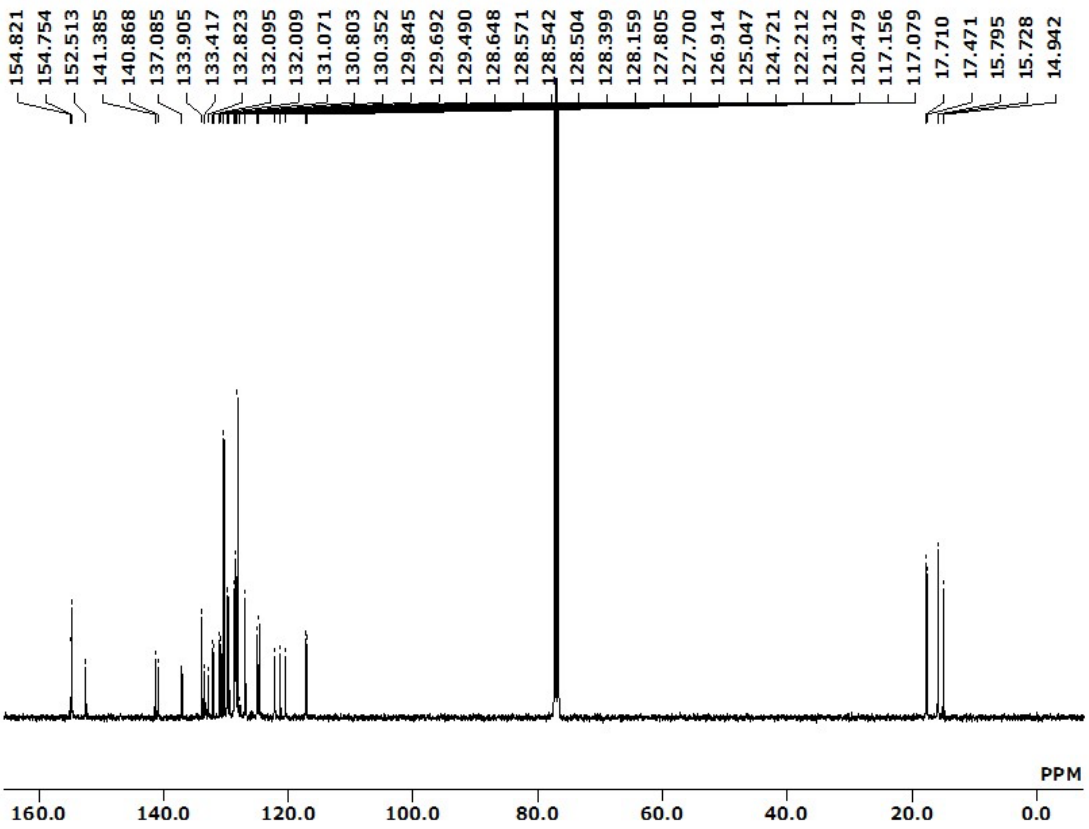

Fig. S5 ^{13}C NMR spectrum of *R*-1Ph-B-BODIPY.

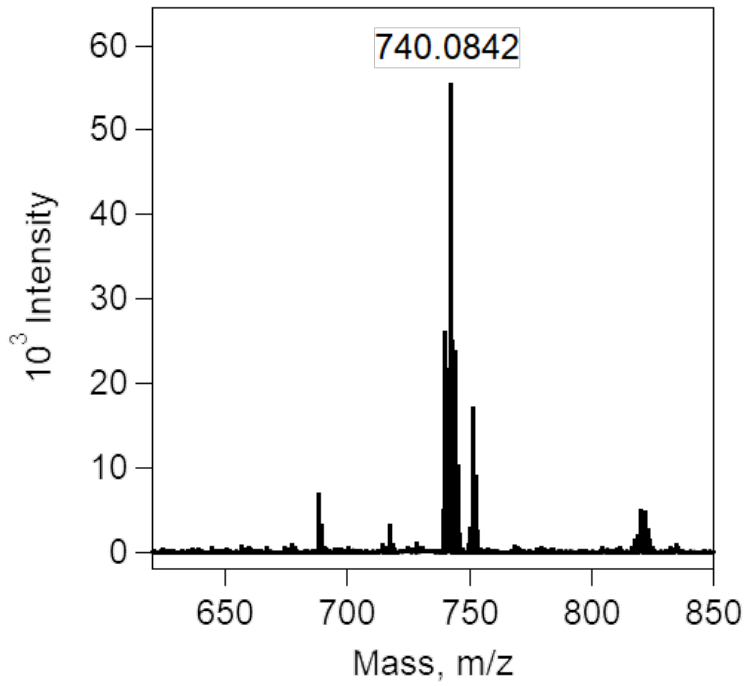

Fig. S6 High resolution MALDI−TOF MS spectrum of *R*-1Ph-B-BODIPY.

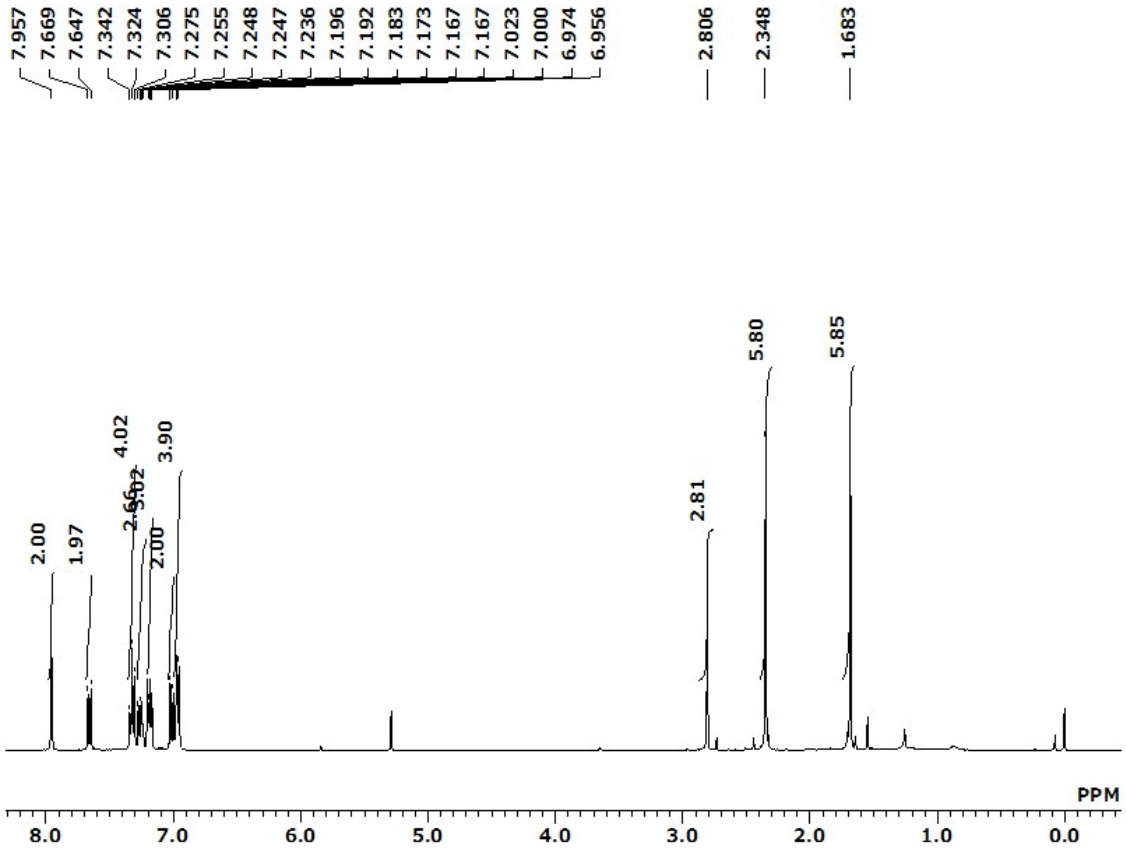

Fig. S7 ^{1}H NMR spectrum of *R*-2Ph-B-BODIPY.

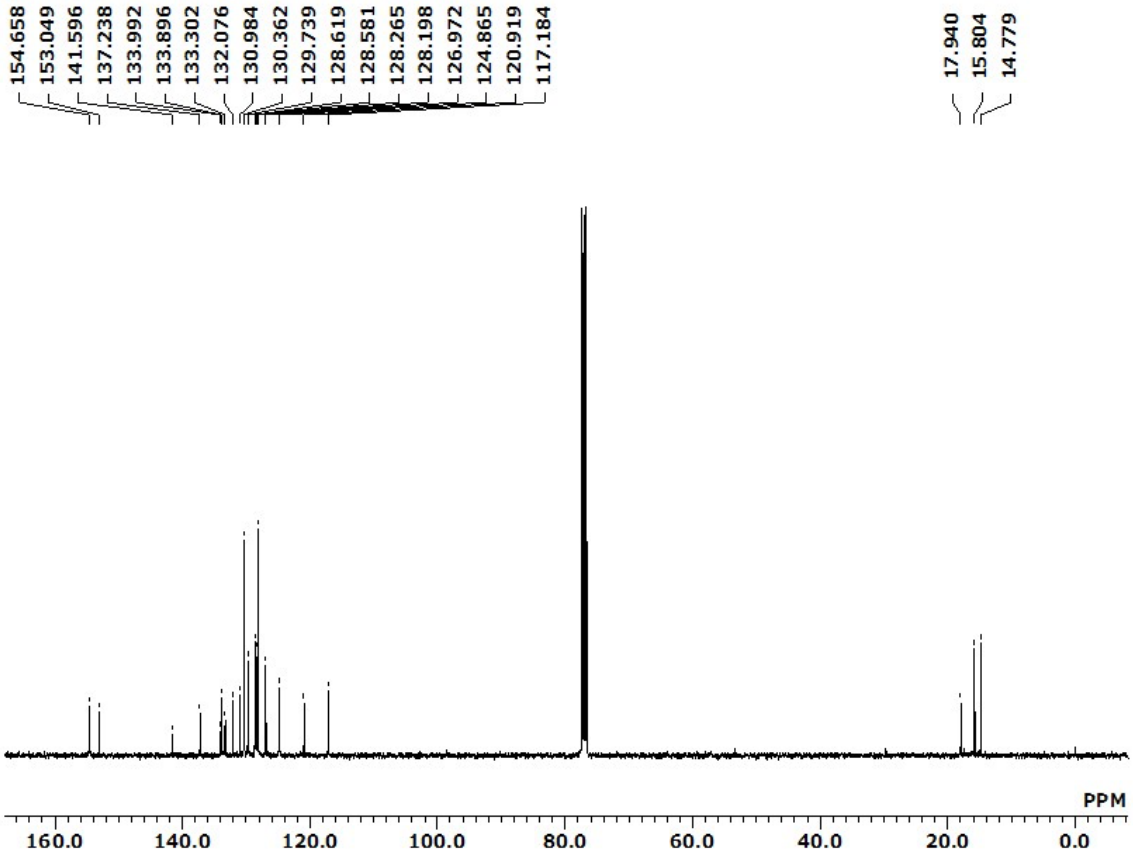

Fig. S8 ^{13}C NMR spectrum of *R*-2Ph-B-BODIPY.

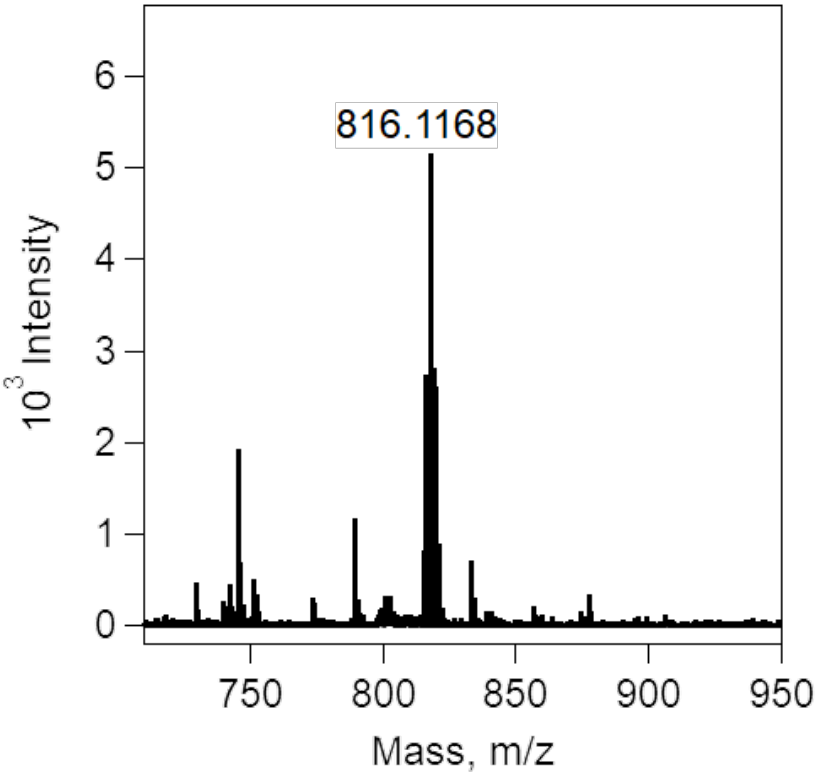

Fig. S9 High resolution MALDI−TOF MS spectrum of *R*-2Ph-B-BODIPY.

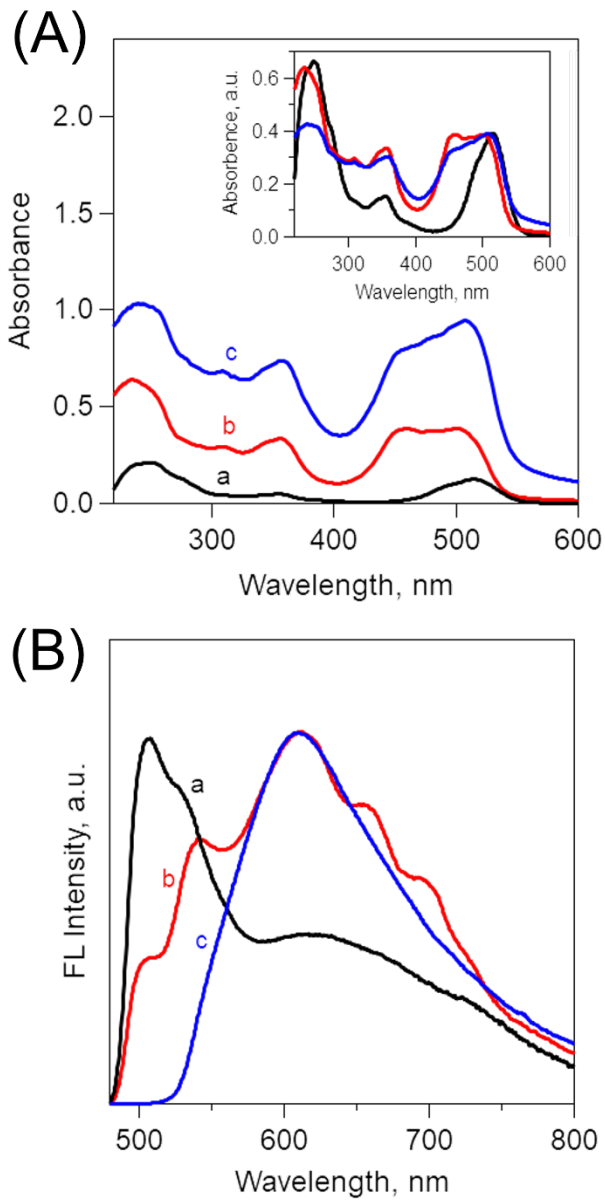

Fig. S10 (A) Concentration-dependent absorption spectra of $(0Ph\text{-}B\text{-}BODIPY)_m$. (a) 3.0 μM, (b) 30 μM, and (c) 300 μM in H_2O/THF = 99/1 (v/v). The insertion figure indicated the normalized spectra for comparison. (B) Concentration-dependent fluorescence spectra of $(0Ph\text{-}B\text{-}BODIPY)_m$, (a) 3.0 μM, (b) 30 μM, and (c) 300 μM. $\lambda_{ex.}$ = 470 nm. We can see a broad fluorescence spectrum derived from molecular aggregation under the experimental condition of 30 μM in H_2O/THF = 99/1 (v/v).

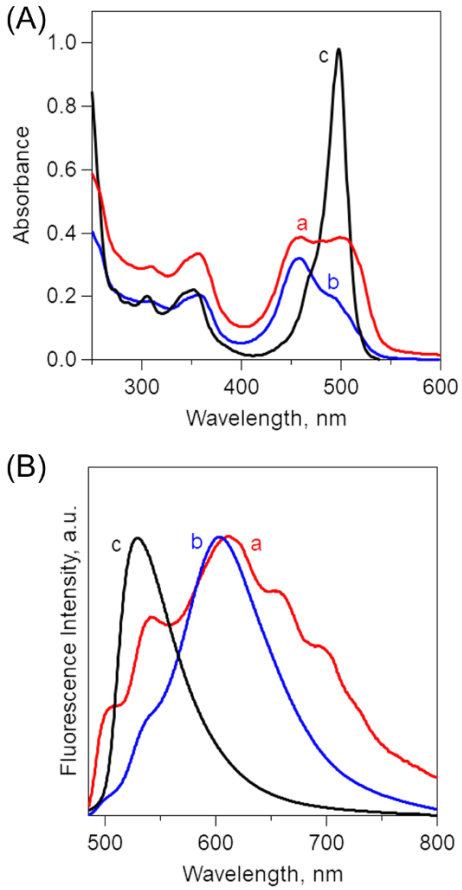

Fig. S11 (A) Absorption spectra of $(0Ph\text{-}B\text{-}BODIPY)_m$ in a mixed solvent of H_2O and THF with different volume ratios. (a) H_2O/THF = 99/1 (v/v), (b) H_2O/THF = 70/30 (v/v), and (c) H_2O/THF = 50/50 (v/v). The final concentrations of 0Ph-B-BODIPY were fixed as constant (= 30 μM). (B) Absorption spectra of $(0Ph\text{-}B\text{-}BODIPY)_m$ in a mixture solvent of THF and water with different ratios. (a) H_2O/THF = 99/1 (v/v), (b) H_2O/THF = 70/30 (v/v), and (c) H_2O/THF = 50/50 (v/v). The final concentration was fixed as constant (= 30 μM). $\lambda_{ex.}$ = 470 nm.

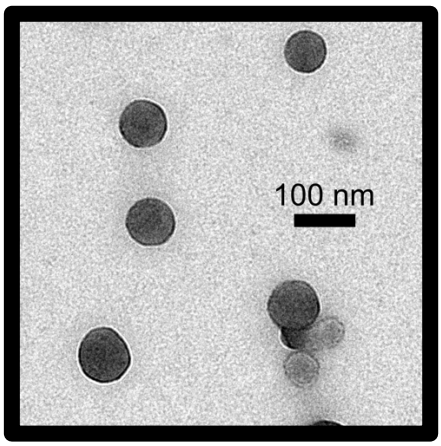

Fig. S12 TEM image of $(0Ph\text{-}B\text{-}BODIPY)_m$ in H_2O/THF = 70/30 (v/v). The final concentration of 0Ph-B-BODIPY was 30 μM in H_2O/THF.

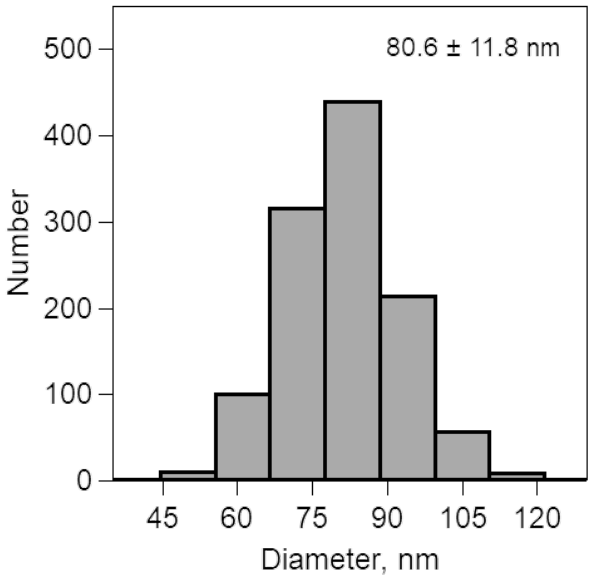

Fig. S13 Diameter-distributions of $(0Ph\text{-}B\text{-}BODIPY)_m$ in H_2O/THF = 70/30 (v/v) analysed by TEM images. The final concentration of 0Ph-B-BODIPY is 30 μM in H_2O/THF.

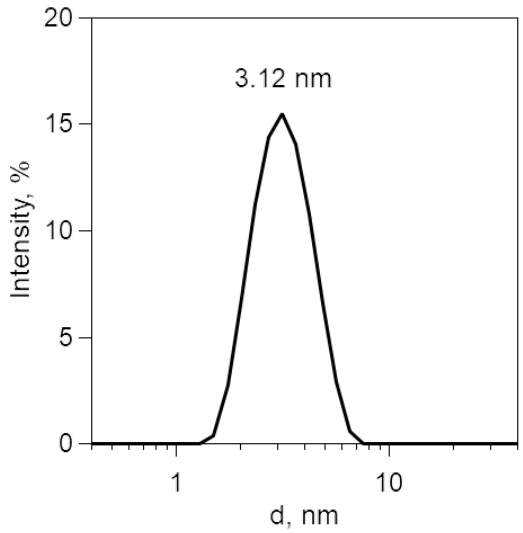

Fig. S14 Size-distributions of $(0Ph\text{-}B\text{-}BODIPY)_m$ in H_2O/THF = 50/50 (v/v) (final concentration of 0Ph-B-BODIPY: [0Ph-B-BODIPY] = 30 μM in H_2O/THF) by dynamic light scattering (DLS) measurements.

To discuss the solvent ratio-dependent structural changes, the following two different $(0Ph\text{-}B\text{-}BODIPY)_m$ systems with volume ratios such as H_2O/THF = 70/30 and 50/50 were prepared by maintaining the final concentrations (30 μM) in mixed solvents. Absorption and fluorescence spectra and TEM images of these systems prepared in H_2O/THF = 70/30 and 50/50 (v/v) are totally different from those prepared in H_2O/THF = 99/1 (v/v) (Figs. S11-S14 in ESI). Isotropic spherical assemblies prepared in H_2O/THF = 70/30 (v/v) (Figs. S12-S13) are in sharp contrast with the anisotropic fibrous assemblies in H_2O/THF = 99/1 (v/v) (Fig. 2A in the text). Furthermore, absorption and fluorescence spectra (Fig. S11) and dynamic light scattering (DLS) result (Fig. S14) in H_2O/THF = 50/50 (v/v) demonstrated a monomer-like behavior, but not aggregate formations (No specific aggregate structures were observed by TEM measurements). Thus, such fibrous assemblies could be fabricated only under the excess volume condition of H_2O relative to THF such as 30 μM 0Ph-B-BODIPY in H_2O/THF = 99/1 (v/v).

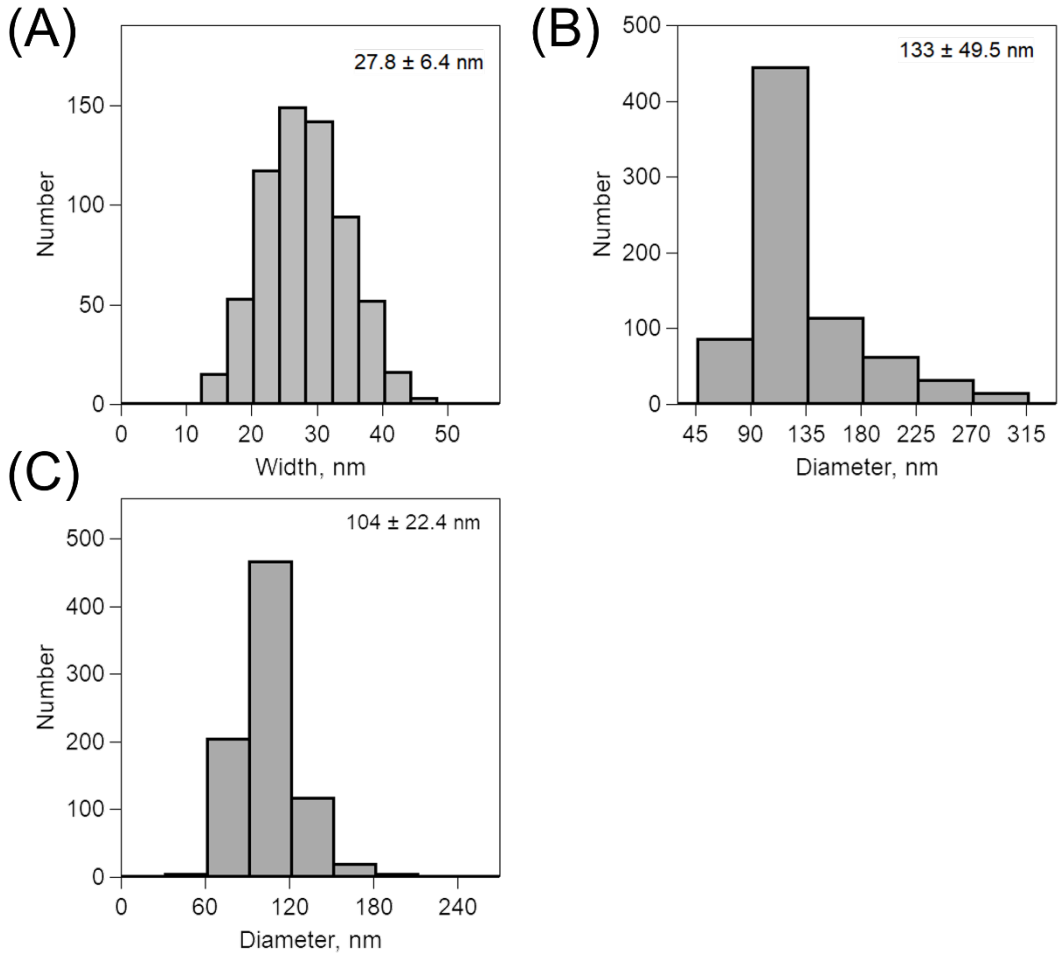

Fig. S15 The width and diameter-distributions of B-BODIPY assemblies. (A) The width-distribution of $(0Ph\text{-}B\text{-}BODIPY)_m$ prepared in H_2O/THF = 99/1 (v/v) ([0Ph-B-BODIPY] = 30 μM), (B) the diameter-distribution of $(1Ph\text{-}B\text{-}BODIPY)_m$ prepared in H_2O/THF = 99/1 (v/v) ([1Ph-B-BODIPY] = 30 μM), and (C) the diameter-distribution of $(2Ph\text{-}B\text{-}BODIPY)_m$ prepared in H_2O/THF = 99/1 (v/v) ([2Ph-B-BODIPY] = 30 μM).

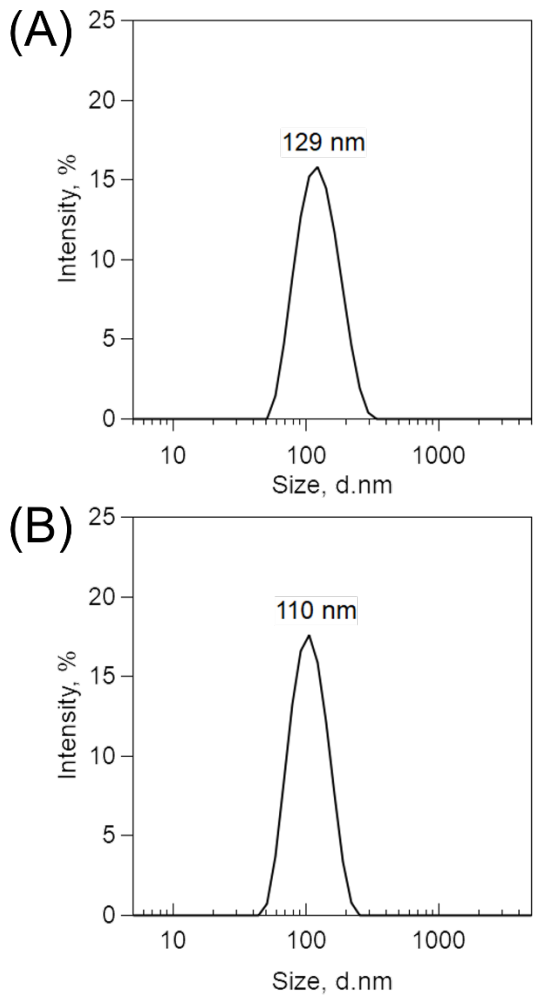

Fig. S16 Size-distributions of (A) $(1Ph\text{-}B\text{-}BODIPY)_m$ prepared in H_2O/THF = 99/1 (v/v) ([1Ph-B-BODIPY] = 30 μM) and (B) $(2Ph\text{-}B\text{-}BODIPY)_m$ prepared in H_2O/THF = 99/1 (v/v) ([2Ph-B-BODIPY] = 30 μM) by dynamic light scattering (DLS) measurements.

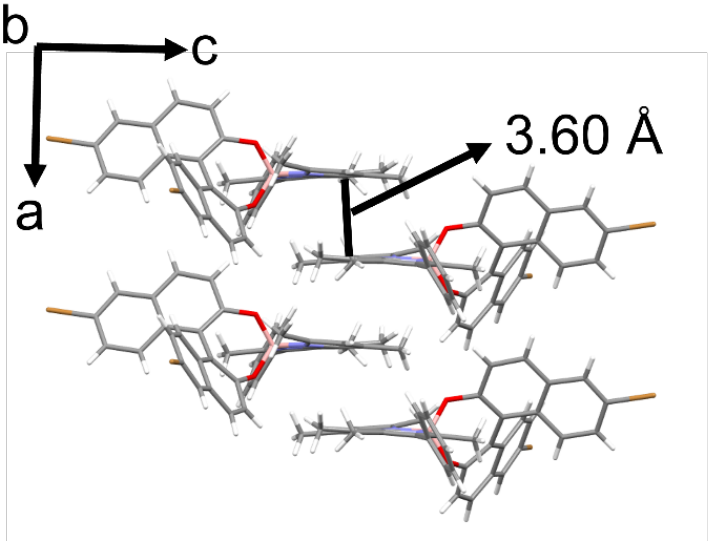

Fig. S17 Single-crystal structures of π-stacking between two neighboring *R*-1Ph-B-BODIPY. Black line: π-stacking distance: 3.60 Å.

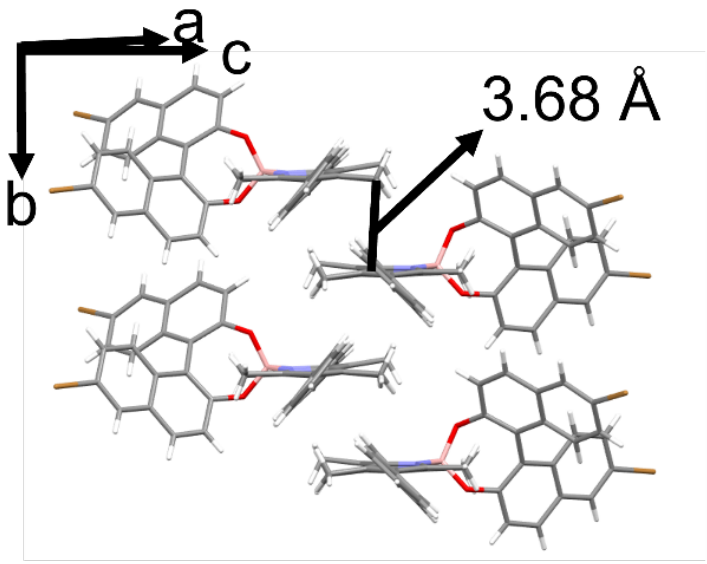

Fig. S18 Single-crystal structures of π-stacking between two neighboring *R*-2Ph-B-BODIPY. Black line: π-stacking distance: 3.68 Å.

Table S1. Single crystal structures and crystallographic data of *R*-0Ph-B-BODIPY.

Compound	*R*-0Ph-B-BODIPY
Formula	$C_{34}H_{27}BBr_2N_2O_2$
Formula Weight	666.22
Crystal System	Orthorhombic
Space Group	$P2_12_12_1$ (#19)
a, Å	6.8301(16)
b, Å	21.461(5)
c, Å	22.842(5)
α, degree	90.0000
β, degree	90.018(6)
γ, degree	90.0000
V, Å^3	3348.2(14)
Z	4
$D_{calc,}$ g cm^{-3}	1.322

Table S2. Single crystal structures and crystallographic data of *R*-1Ph-B-BODIPY.

Compound	*R*-1Ph-B-BODIPY
Formula	$C_{46}H_{45}BBr_2N_2O_2$
Formula Weight	828.49
Crystal System	Orthorhombic
Space Group	$P2_12_12_1$ (#19)
a, Å	6.7759(3)
b, Å	22.5581(11)
c, Å	26.3420(13)
α, degree	90.0000
β, degree	90.0000
γ, degree	90.0000
V, Å^3	4026.4(3)
Z	4
$D_{calc,}$ g cm^{-3}	1.367

Table S3. Single crystal structures and crystallographic data of *R*-2Ph-B-BODIPY.

Compound	*R*-2Ph-B-BODIPY
Formula	$C_{46}H_{35}BBr_2N_2O_2$
Formula Weight	818.41
Crystal System	Monoclinic
Space Group	$P2_1$ (#4)
a, Å	14.0582(3)
b, Å	7.39498(13)
c, Å	17.5218(3)
α, degree	90.0000
β, degree	93.311(7)
γ, degree	90.0000
V, Å^3	1818.53(6)
Z	2
$D_{calc,}$ g cm^{-3}	1.495

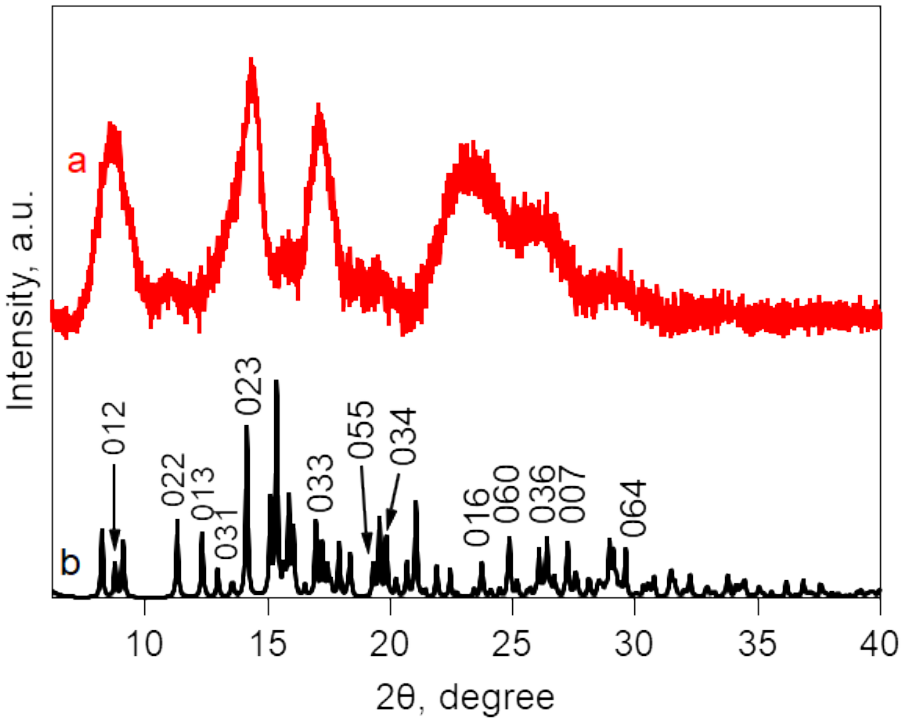

Fig. S19 XRD patterns of (a) $(0Ph\text{-}B\text{-}BODIPY)_m$ prepared in H_2O/THF = 99/1 (v/v) and (b) a simulated pattern from the crystal structure of 0Ph-B-BODIPY.

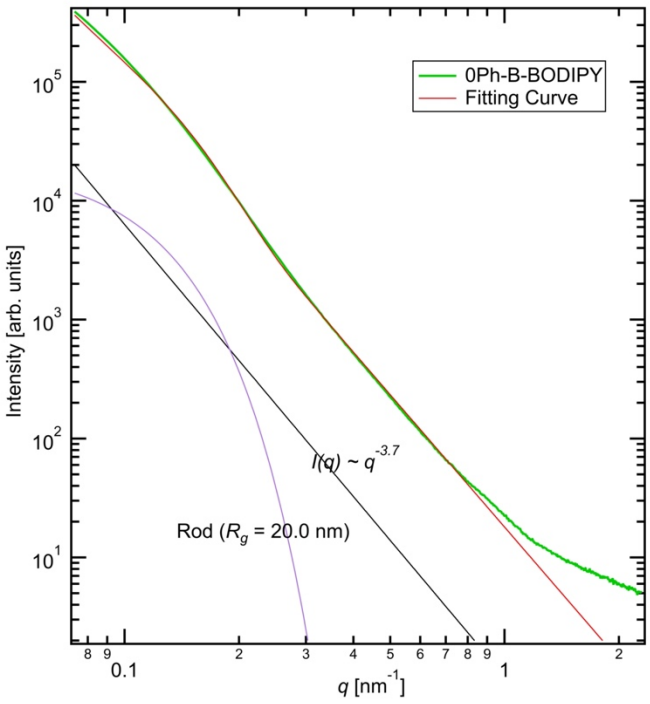

Fig. S20 Small-angle X-ray scattering (SAXS) profile of $(0Ph\text{-}B\text{-}BODIPY)_m$ prepared in H_2O/THF = 99/1 (v/v).

In SAXS profile of $(0Ph\text{-}B\text{-}BODIPY)_m$, we fitted the profile with eq. (2), which is based on the cross-section plot, a method for analyzing fibrous aggregates.

$$I(q) = aq^{-3.7} + be^{-\frac{1}{2}q^2R_1^2} \qquad (2)$$

Here, $I(q)$ is scattering intensity, a, and b are constant, q is scattering angle, and R_1 is radius of gyration for rods. The profile in the low-q region is described by $I(q) \sim q^{-3.7}$. The scattering profile originates from the smooth interface owing to the surface dimension of 2.3. This interface is believed to be derived from micron-scaled particles. Eq. (2) could be fitted to the profile, and SAXS data also suggested fibrous assemblies of $(0Ph\text{-}B\text{-}BODIPY)_m$. Consequently, R_1 was calculated to be 20.0 nm, which is comparable to the width value in TEM image (Fig.2A and Fig. S11A in ESI†).

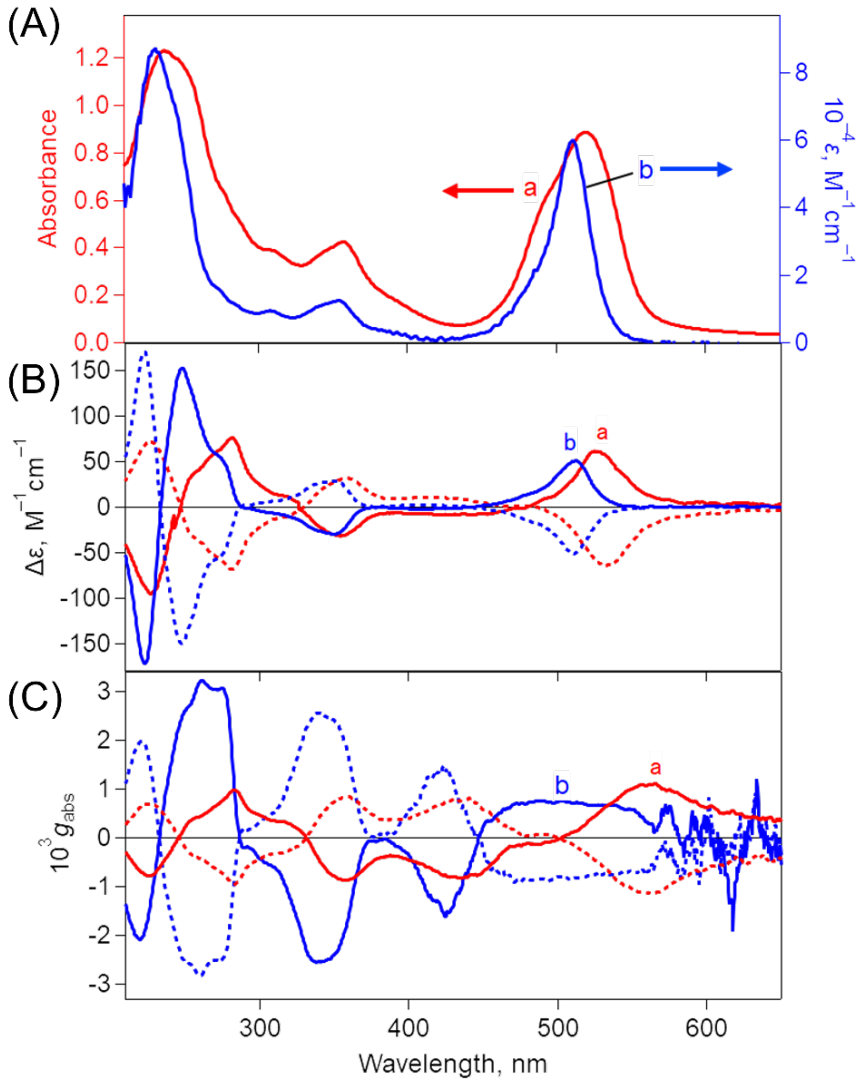

Fig. S21 (A) Absorption spectra of (a) $(1Ph\text{-}B\text{-}BODIPY)_m$ prepared in H_2O/THF = 99/1 (v/v). [1Ph-B-BODIPY] = 30 μM and (b) 1Ph-B-BODIPY in THF. (B) CD spectra of (a) $(1Ph\text{-}B\text{-}BODIPY)_m$ prepared in H_2O/THF = 99/1 (v/v). [1Ph-B-BODIPY] = 30 μM and (b) 1Ph-B-BODIPY in THF. Solid and dotted lines correspond to *S* and *R* forms, respectively. (C) Dissymmetry factor (g_{abs}) profiles of (a) $(1Ph\text{-}B\text{-}BODIPY)_m$ prepared in H_2O/THF = 99/1 (v/v). [1Ph-B-BODIPY] = 30 μM and (b) 1Ph-B-BODIPY in THF. Solid and dotted lines correspond to *S* and *R* forms, respectively.

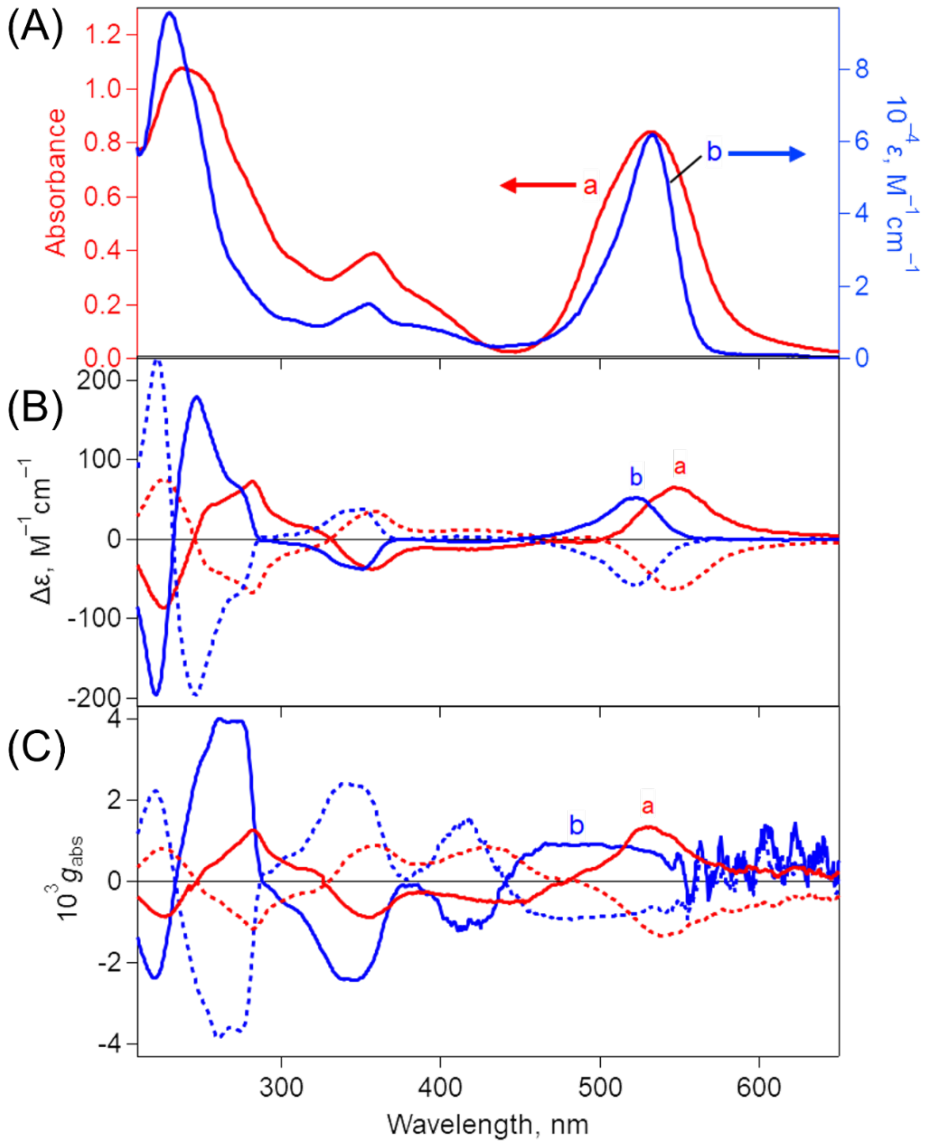

Fig. S22 (A) Absorption spectra of (a) $(2Ph\text{-}B\text{-}BODIPY)_m$ prepared in H_2O/THF = 99/1 (v/v). [2Ph-B-BODIPY] = 30 μM and (b) 2Ph-B-BODIPY in THF. (B) CD spectra of (a) $(2Ph\text{-}B\text{-}BODIPY)_m$ prepared in H_2O/THF = 99/1 (v/v). [1Ph-B-BODIPY] = 30 μM and (b) 2Ph-B-BODIPY in THF. Solid and dotted lines correspond to *S* and *R* forms, respectively. (C) Dissymmetry factor (g_{abs}) profiles of (a) $(2Ph\text{-}B\text{-}BODIPY)_m$ prepared in H_2O/THF = 99/1 (v/v). [2Ph-B-BODIPY] = 30 μM and (b) 2Ph-B-BODIPY in THF. Solid and dotted lines correspond to *S* and *R* forms, respectively.

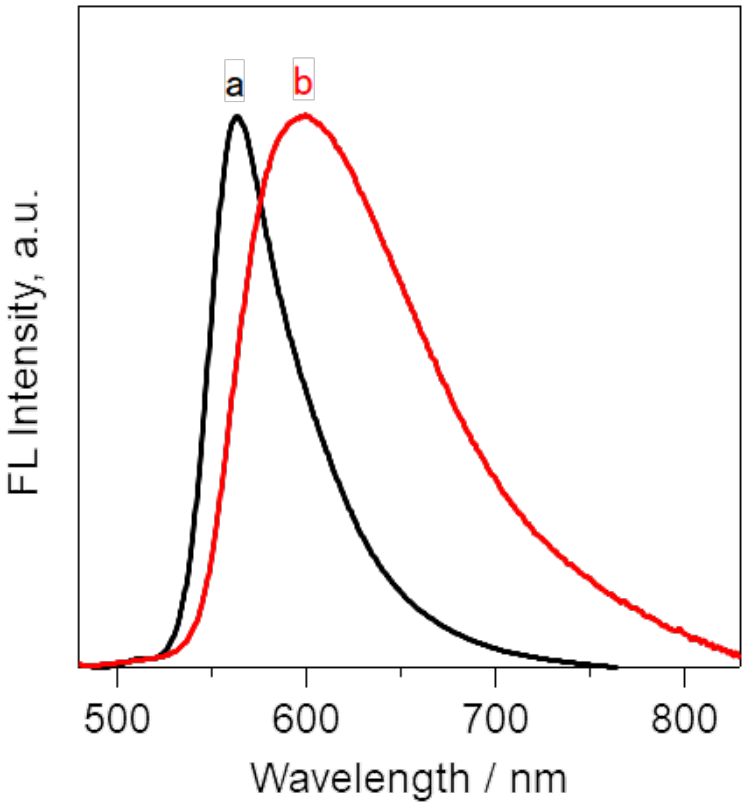

Fig. S23 Fluorescence spectra of (a) 2Ph-B-BODIPY (monomer: black line) in THF and (b) $(2Ph\text{-}B\text{-}BODIPY)_m$ (red line) prepared in H_2O/THF = 99/1 (v/v). λ_{ex}: 470 nm.

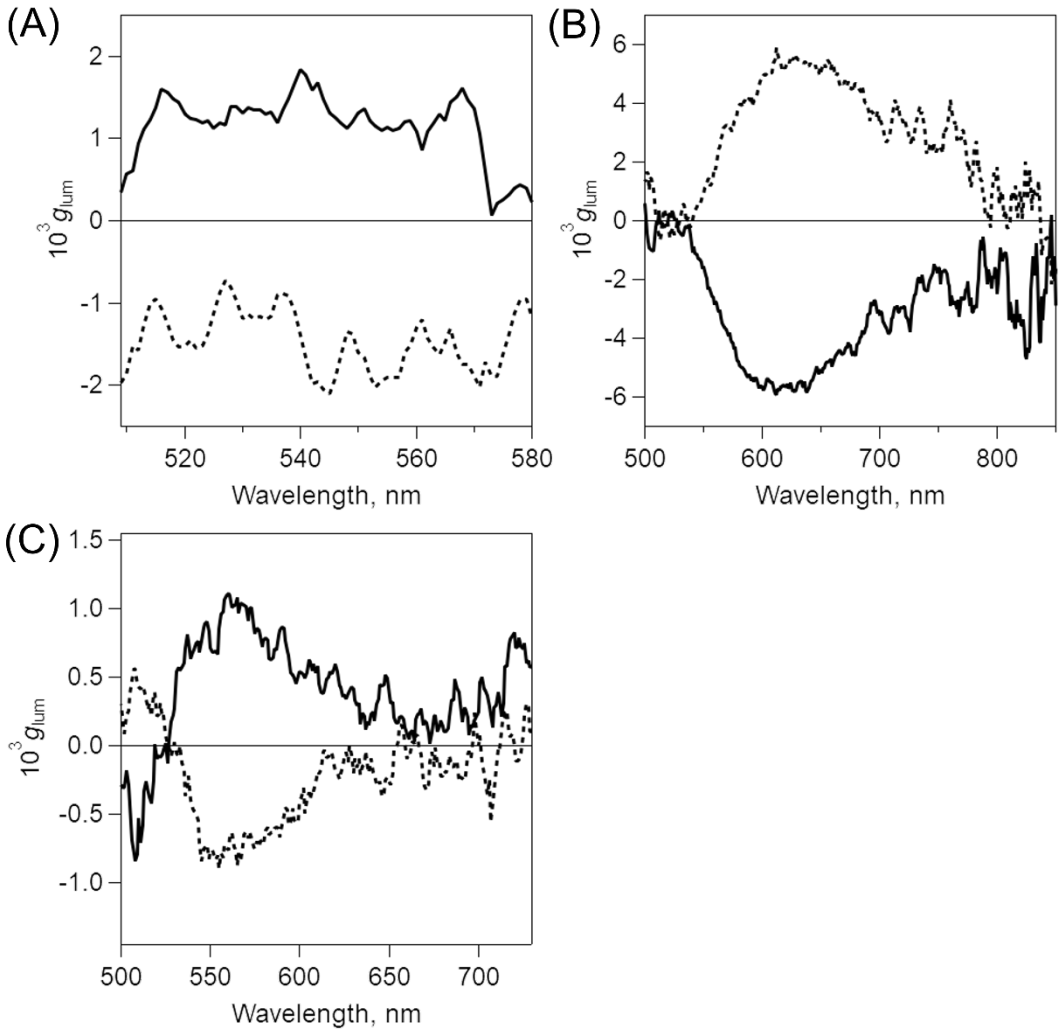

Fig. S24 Dissymmetry factor (g_{lum}) profiles corresponding to CPL spectra of (A) 0Ph-B-BODIPY (monomer) in THF, λ_{ex}: 350 nm. (B) $(0Ph\text{-}B\text{-}BODIPY)_m$ prepared in H_2O/THF = 99/1 (v/v), λ_{ex}: 350 nm. (C) $(1Ph\text{-}B\text{-}BODIPY)_m$ prepared in H_2O/THF = 99/1 (v/v), λ_{ex}: 350 nm. Solid and dotted lines correspond to *S* and *R* forms, respectively.

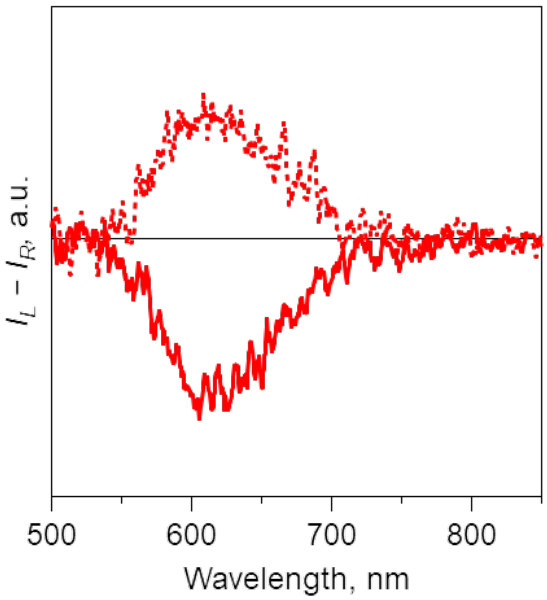

Fig. S25 CPL spectra of $(0Ph\text{-}B\text{-}BODIPY)_m$ prepared in H_2O/THF = 70/30 (v/v). [0Ph-B-BODIPY] = 30 μM, λ_{ex}: 350 nm. Solid and dotted lines correspond to *S* and *R* forms, respectively.

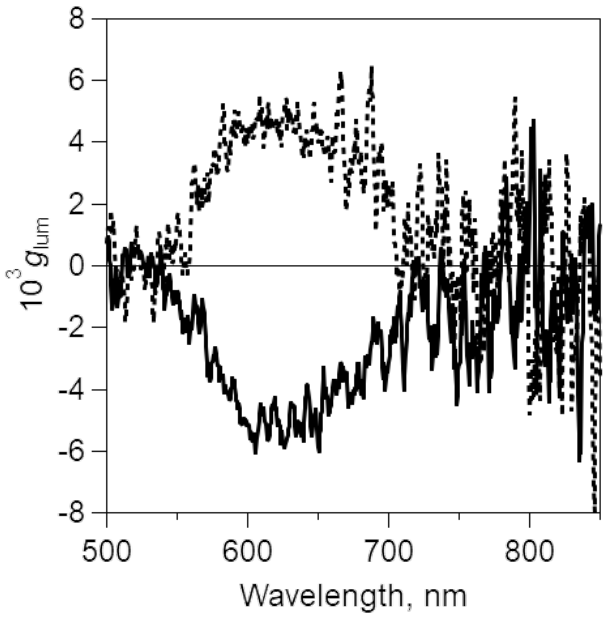

Fig. S26 Dissymmetry factor (g_{lum}) profiles corresponding to CPL spectra of (0Ph-B-BODIPY)$_m$ prepared in H_2O/THF = 70/30 (v/v). [0Ph-B-BODIPY] = 30 μM, λ_{ex}: 350 nm. Solid and dotted lines correspond to *S* and *R* forms, respectively.

(0Ph-B-BODIPY)$_m$ prepared in H_2O/THF = 70/30 (v/v) demonstrated broader CPL spectra relative to the monomers, whereas the corresponding g_{lum} value slightly decreased as compared to that in H_2O/THF = 99/1 (v/v) (Figs.S25 and S26). The plausible reason is attributable due to the relative weak interaction between nearby 0Ph-B-BODIPY molecules. In contrast, in the case of (0Ph-B-BODIPY)$_m$ prepared in H_2O/THF = 50/50 (v/v), unfortunately we could not observe appropriate CPL spectra despite the repeated measurements due to the unstable suspension of (0Ph-B-BODIPY)$_m$ in H_2O/THF. This strongly suggested that the excess volume condition of H_2O (poor solvent) relative to THF (good solvent) (e.g., H_2O/THF = 99/1 (v/v)) play an important role for preparation of stable aggregate structures.